Journal of Advanced Ceramics
2012, 1(4): 327-335
DOI: 10.1007/s40145-012-0033-x ISSN 2226-4108

Research Article

Synthesis and characterization of $Zr_{0.85}Y_{0.15}O_{1.925}$-$La_{9.33}Si_6O_{26}$ composite electrolyte for application in SOFCs

Chaofeng LIU[a], Hong ZHANG[a], Junxiao XIA[a], Zhicheng LI[a,b,*]

[a] *School of Materials Science and Engineering*, *Central South University*, *Changsha 410083*, *China*
[b] *State Key Laboratory of Powder Metallurgy*, *Central South University*, *Changsha 410083*, *China*

Received: November 16, 2012; Revised: December 9, 2012; Accepted: December 11, 2012

Abstract: Composite oxide ionic conductors consisting of $Zr_{0.85}Y_{0.15}O_{1.925}$ (YSZ) and $La_{9.33}Si_6O_{26}$ (LSO) have been synthesized by a modified coprecipitation method. X-ray diffraction, electron microscope, and complex impedance were adopted to investigate the phase component, microstructures, and conductivities, respectively. The results show that the average grain sizes of the composite powders and as-sintered pellets are less than 20 nm and 200 nm, respectively. The conductivity of the composite materials composed of 94 wt% YSZ and 6 wt% LSO is 0.215 S/cm at 700 ℃. The conductivity of the composite is three times higher than that of the polycrystalline YSZ and has two orders in magnitude higher than that of the polycrystalline LSO at 700 ℃. By analyzing the impedance spectra and modulus spectra, the grain-boundary effect on the conductivity improvement is investigated and the conductive mechanisms of the composite materials are discussed.

Key words: $Zr_{0.85}Y_{0.15}O_{1.925}$; $La_{9.33}Si_6O_{26}$; composite materials; coprecipitation synthesis; oxygen ionic conductivity

1 Introduction

Solid oxide fuel cell (SOFC), which is a device converting directly the chemical energy of fuels such as hydrogen, methanol, ethanol, and methane energies into electrical energy, has several merits over direct combustion devices, including higher efficiency, lower or zero emission, and higher power density [1]. With the increasing concerns of the global warming and pollution resulted from the exhaust of fossil fuels, tremendous effort has been put into research and development of SOFCs during the last decades. However, the operating temperatures of the commercial SOFCs with the electrolyte of yttria stabilized zirconia (YSZ) are 900-1000 ℃ when the requirement of oxygen-ionic conductivity is higher than 0.1 S/cm. At high operating temperature, some harsh terms such as the sealing problem, thermal matches between materials and interface interaction between electrolyte and electrodes, etc., could be met, leading to higher manufacturing costs and application limitation for SOFC. To develop the intermediate temperature (IT) SOFCs (operating at 500-700 ℃), the improvement of oxygen-ionic conductivity of electrolytes is becoming one of the most important topics.

* Corresponding author.
E-mail: zhchli@csu.edu.cn

In general, there are two possible ways to get a higher conductivity electrolyte, i.e., to find a new type of oxygen ionic conductor and to modify the microstructure of the present oxygen ionic conductors. The former is a complex work for that it is not easy to find a new suitable compound. The composite process and nano-technology were reported to be the effective ways to improve dramatically the oxygen-ionic conductivity [2-9]. The conductivities of the composite materials consisting of the doped ceria and lanthanum silicate could be enhanced obviously by a nanocomposite process [2]. The oxygen ionic conductivity of nano-structured layer-by-layer electrolytes composed of gadolinia-doped ceria and zirconia could be increased greatly [4]. In YSZ-$SrTiO_3$ epitaxial heterostructures, a high lateral oxygen ionic conductivity, showing up to eight orders of magnitude enhancement near room temperature, was reported [6]. Superionic conductivities are observed for epitaxial YSZ films on MgO substrate because interfacial effects dominate the conductivity [7]. The composite materials composed of doped lanthanum gallate and doped ceria could not only enhance the conductivities, but also the properties of the cells could be obviously improved when the composite material was used as electrolyte [10]. The work by Chockalingam *et al*. revealed that nanocomposite with doped ceria and alumina had an impressive conductivity (0.316 S/cm at 700 ℃) [11]. It is reported that Al_2O_3 shows a beneficial effect on sintering behaviour and mechanical properties of Y_2O_3-doped CeO_2 [9]. These indicate that composite or nanocomposite technology will evoke a new research tendency for the development of solid electrolytes for SOFCs.

The YSZ electrolyte has high ionic conductivity and ionic transference number as well as good mechanical property at elevated temperatures. The conductivities of YSZ with 8 mol% Y_2O_3 are 0.16 S/cm at 1000 ℃ and 0.027 S/cm at 800 ℃ [12,13]. Meanwhile, the apatite-type lanthanum silicates such as $La_{9.33}Si_6O_{26}$ (LSO) exhibit high chemical and structural stability at high temperatures, and have high oxygen ion transference number over a wide range of oxygen partial pressures [14-17]. The investigation of the apatite lanthanum silicates has attracted much attention recent years, although the ionic conductivity needs to be improved further.

Although YSZ and LSO have some novel characteristics, their conductivities are not high enough for the application in IT-SOFCs. To our knowledge, there has not been any report on the composite oxygen ionic conductor consisted of YSZ and LSO so far. In present paper the $Zr_{0.85}Y_{0.15}O_{1.925}$-$La_{9.33}Si_6O_{26}$ (YSZ-LSO) composite materials were prepared and the results show that the conductivities could be improved obviously by the composite technique.

2 Experimental procedure

Appropriate amounts of zirconium (IV) oxide chloride ($ZrOCl_2{\cdot}8H_2O$, >98%, Dahao Shantou, China) and yttria (Y_2O_3, 99.99%, Yuejing Shanghai, China) were mixed according to the formula of YSZ and dissolved into dilute nitric acid. The mixed solution was dropped into dilute ammonia solution (pH~8) under vigorous stirring. After being aged at 50 ℃ for 12 h, the precursor was repeatedly centrifuged with distilled water and alcohol until the chlorine ions were eliminated completely. Citric acid ($C_6H_8O_7$, AR, Hengxing Tianjin, China) and Polyethylene glycol (PEG-400, CP, Youji Changsha, China) were added into the precipitate and the colloid was ultrasonically dispersed. Then the dispersed precursors were dried by stirring and heating. The dried precursors were calcined at 800 ℃ for 60 min to obtain YSZ powders.

On the other hand, according to the formula of LSO, appropriate amount of lanthanum oxide (La_2O_3, 99.9%, Xilong Guangdong, China) was dissolved into dilute nitric acid, and tetraethoxysilane (TEOS, AR, Xilong Guangdong, China) was dissolved into alcohol. Then the two clear solutions were mixed. This mixed solution was dropped into dilute ammonia solution (pH~8) under vigorous stirring. Then polyethylene glycol and critic acid were added to modify the surface of precipitate and to disperse them. After being aged at 50 ℃ for 12 h, the precursors were dried by stirring and heating. The dried precursors were calcined at 850 ℃ for 60 min to obtain LSO powders.

To prepare the composite materials, two batches with the LSO to YSZ weight ratios of 4 to 96 and 6 to 94 were designed (recorded as YSZ-4LSO and YSZ-6LSO, respectively). According to the weight ratios, LSO powder and YSZ powder were weighted and mixed in alcohol-water solution (volume ratio of alcohol-water, 1 : 1). 10 ml polyvinyl alcohol (PVA, >99%, Kermel, Tianjin, China) solution, containing 0.15 g PVA, was added to disperse the powders. The

mixtures were stirred for 24 h and then were dried to obtain the YSZ-4LSO and YSZ-6LSO composite powders.

The single phase powders and composite powders were axially pressed under 100 MPa to get green pellets with 10 mm in diameter and about 4 mm in thickness. The green pellets of YSZ-4LSO and YSZ-6LSO composite were sintered at 1400 ℃ for 120 min, and YSZ and LSO green pellets were sintered at 1500 ℃ for 120 min, with a heating/cooling rate of 5 ℃/min. The densities of the as-sintered ceramics were measured with Archimedes principle. As a result, all the studied ceramics have similar relative densities of 92.18%-93.0%.

Phase identification was performed by using X-ray diffraction (XRD) (D/Max 2500, Japan) with Cu K_α radiation (λ=1.5406 Å) at room temperature. The mean crystallite size was determined by using Scherer formula ($D=k\lambda/\beta\cos\theta$, k=0.89). The calcined powders and as-sintered pellets were investigated by using a transmission electron microscopy (TEM) (Tecnai G^2 20) operating at 200 kV and a scanning electron microscopy (SEM) (FEI SIRION200), respectively. The samples for TEM observation were crushed in an agate mortar, dispersed in ethanol, and deposited onto a holy carbon film microgrid. The samples for SEM observations were first ground, polished, and then thermally etched at 1200 ℃ for 30 min, After being ultrasonic cleaning, the samples were coated with Pt for conductivity reason in the SEM.

The as-sintered samples were ground to thickness about 1 mm. The electrodes were prepared by brushing silver paste onto the both sides of the pellets. The conductivities were determined by using AC impedance measurement (Gamry Reference 600, USA). For impedance measurement, an AC voltage of 50 mV was applied to the sample over a frequency range from 1 MHz to 1 Hz at various temperatures. The conductivity, σ, can be calculated with $\sigma=L/RA$, where L is the sample thickness, A is the electrode area, and R is the resistance as determined with the impedance spectroscopy. The plots of frequency dependence of impedance and the frequency dependence of modulus were carried out using Zview software (Scribner Associates, Inc., Southern Pines, NC). For a clear comparison, all the impedance spectra were scaled according to its maximum.

3 Results and discussion

3.1 Microstructure analysis

Figure 1(a) shows the XRD patterns of the as-calcined powders of YSZ and LSO. The diffraction peaks exhibit that YSZ has a cubic structure and LSO has a hexagonal apatite-type structure. Each of the YSZ and

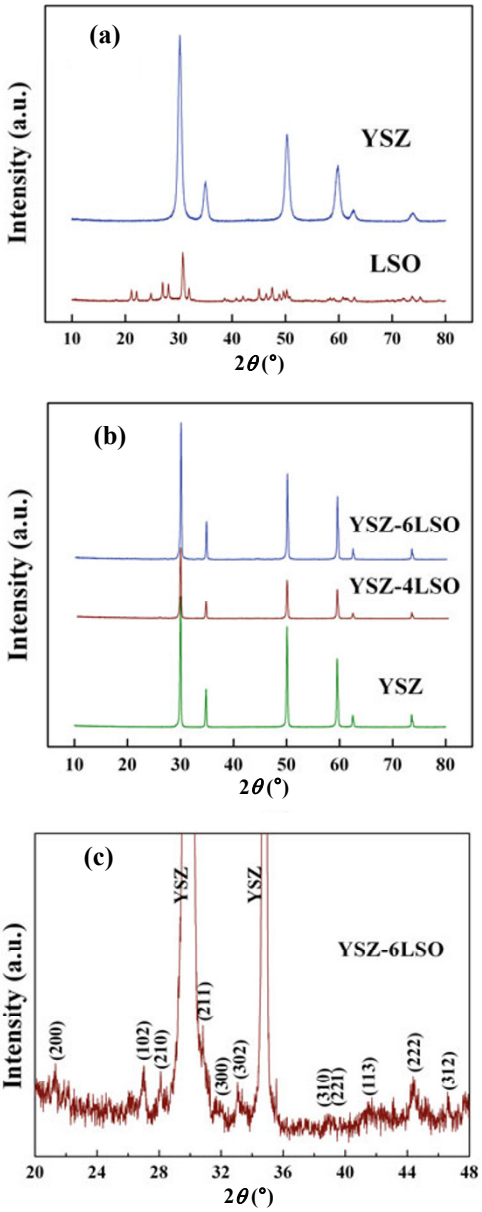

Fig. 1 XRD patterns of the prepared materials, (a) as-calcined powders of YSZ and LSO; (b) as-sintered ceramics of YSZ, YSZ-4LSO and YSZ-6LSO; (c) enlarged diffraction pattern of the diffraction region 2θ = 20°-50° of the YSZ-6LSO.

LSO powders shows a pure single phase. The average grain sizes of the as-calcined powders of YSZ and LSO are calculated by the Scherer formula to be 11.7 nm and 34.8 nm, respectively. These suggest that the powder preparation process is appropriate and effective. Because PEG and Citric acid not only disperse precipitate colloid by steric hindrance effect in liquid phase, but also they act as combustion fuel during the heating process [18]. These processes could eliminate the particles agglomeration. Therefore, the powders with fine grains were obtained.

Figure 1(b) shows the XRD patterns of the as-sintered ceramics of YSZ, YSZ-4LSO and YSZ-6LSO. It is easily found that the main phase of each ceramic is cubic structure. For the YSZ-4LSO and YSZ-6LSO ceramics, the diffraction peaks from the LSO phase are not easy to be detected in Fig. 1(b), because of the small amount of LSO. In order to detect the diffraction peaks of LSO phase, the diffraction pattern of the YSZ-6LSO (range 2θ: 20°-48°) was enlarged and shown in Fig. 1(c). One can see that, besides the peaks from YSZ, the indexed peaks from LSO phase can also be detected. These indicate that the as-sintered composite ceramics are composed of YSZ and LSO phases.

Figure 2(a) is a TEM observation of the as-calcined

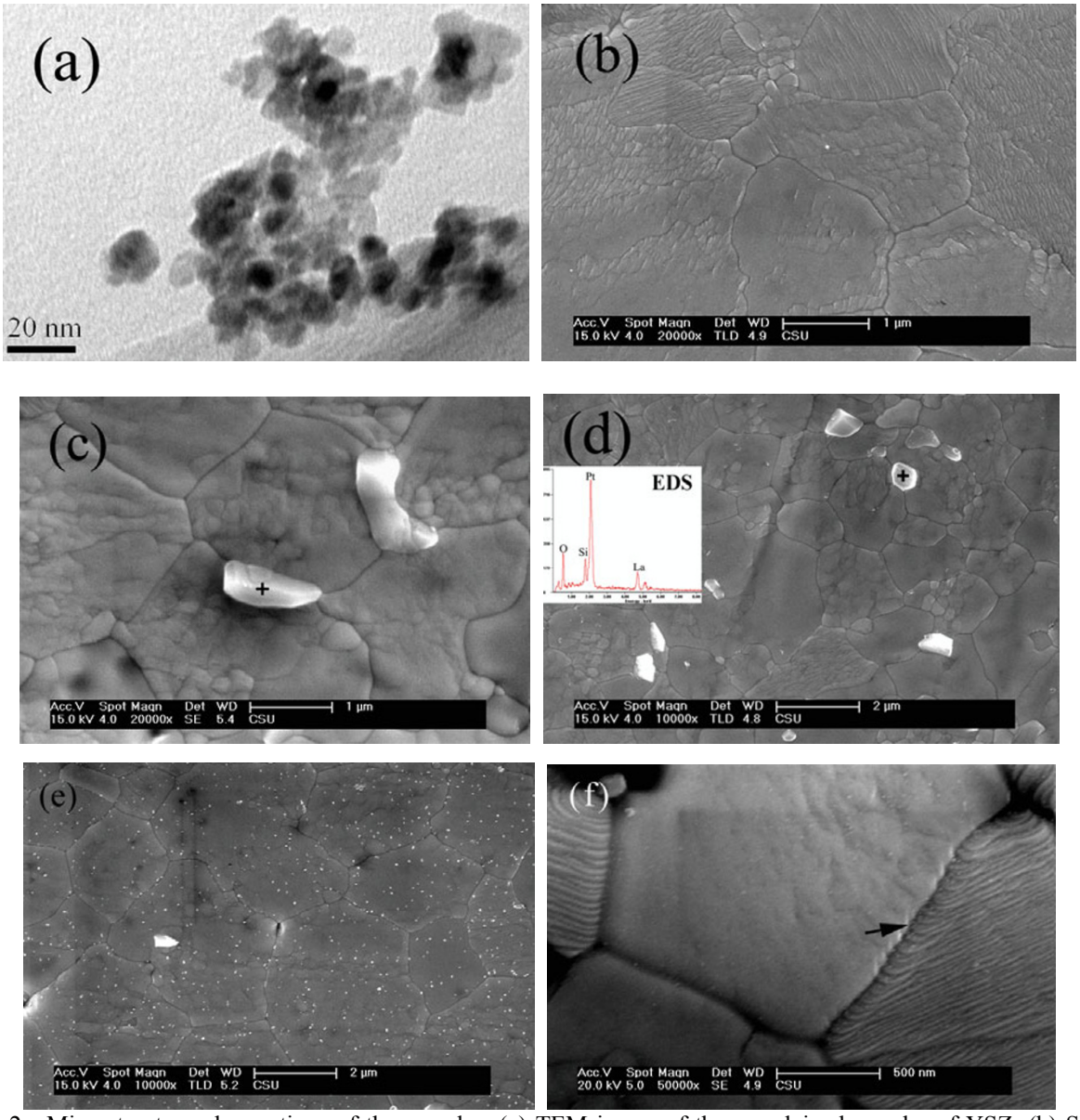

Fig. 2 Microstructure observations of the samples, (a) TEM image of the as-calained powder of YSZ; (b) SEM image of the as-sintered YSZ; (c) SEM image of the as-sintered YSZ-4LSO; (d) SEM image of the as-sintered YSZ-6LSO, and the inset is the EDS spectrum; (e) and (f) SEM image of the as-sintered YSZ-6LSO.

YSZ powder. It can be seen that the average particle size of the powder is around 10 nm. The size is in agreement with the one calculated by Scherrer formula from the XRD spectrum in Fig. 1(a). The SEM photographs of all sintered samples are shown in Figs. 2(b)-2(d). The size of all grains is around 1-2 μm and each grain consists of many sub-grains. The YSZ ceramic in Fig. 2(b), is well densed and the average sub-grain size of the as-sintered ceramic is around 200 nm. The SEM images taken from the YSZ-LSO composite ceramics are shown in Figs. 2(c) and 2(d). The ceramics have two kinds of grains in different colors, most of them are in grey color and few of them are white. The chemical composition of the white color grains marked with "+" in Figs. 2(c) and 2(d) was analyzed by using an energy dispersive X-ray spectrometer (EDS). The EDS result, shown as the inset in Fig. 2(d), display that the kind of white color grain is mostly composed of La, Si, and O elements. Where, the element Pt was from the coating on the surface to increase the electrical conductivity for the SEM observation. Combined with the XRD results, it indicates that the white color grains should belong to the LSO phase. The LSO phase locates at the grain boundaries (see in Fig. 2(f)) or inside of grains of the main phase (see in Fig. 2(e)).

3.2 Conductivity analysis

AC impedance measurements were conducted on the samples at temperatures from 300 ℃ to 700 ℃. Generally, impedance plots of an oxygen-ion conductor exhibit three parts, the arc attributed to bulk effect at high frequency region, the one from the grain boundary effect at intermediate frequencies, and the electrode behavior at low-frequency region. For comparing, the complex impedance spectra of the YSZ ceramic, LSO ceramic, and the YSZ-LSO composite ceramics measured at 300 ℃, 400 ℃ and 500 ℃, respectively, are selected and showed in Fig. 3. The other spectra have the similar phenomenon and are not showed here. At 300 ℃ and 400 ℃, as shown in Figs. 3(a) and 3(b), three parts in the impedance spectrum of each sample can be distinguished for the bulk effect, grain-boundary effect and electrode one, respectively. From the real part of the impedance spectra measured

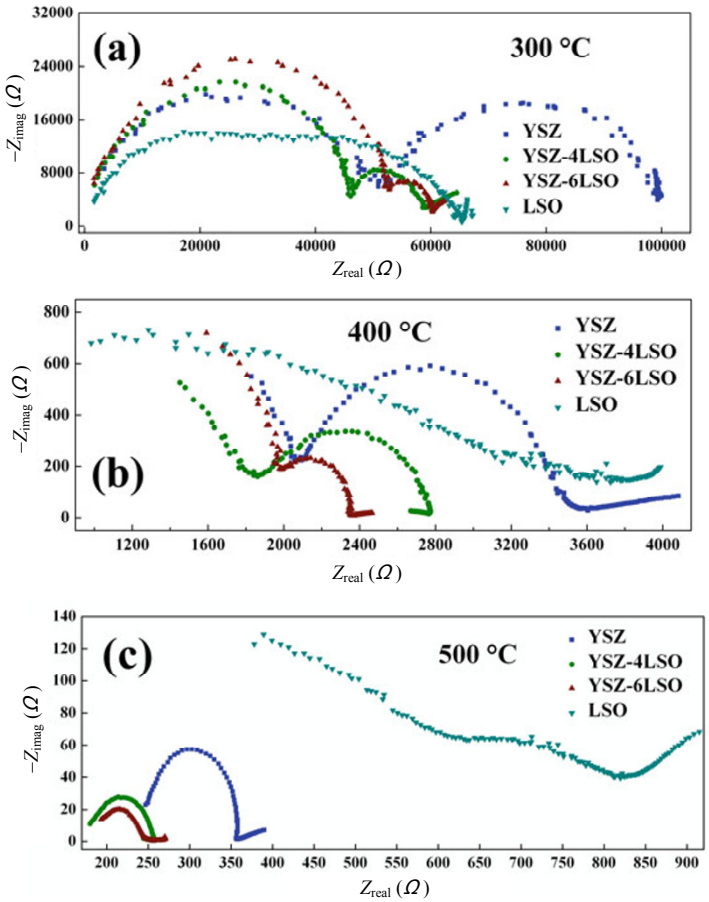

Fig. 3 Complex impedance spectra of the various samples measured at (a) 300 ℃, (b) 400 ℃ and (c) 500 ℃.

at 300 ℃ as shown in Fig. 3(a), one can get that the YSZ or LSO single phase ceramic has the approximate conductivity values from the grain (bulk) effect and the grain boundary effect. For YSZ-LSO composite ceramics, the impedance value from the grain effect is almost the same as that of YSZ or LSO single phase ceramic, but their grain-boundary effect is about one fourth of that of the YSZ or LSO single phase ceramic. This means that the YSZ-LSO composite ceramics have much smaller impedance from the grain-boundary effect. At 400 ℃, as shown in Fig. 3(b), all the samples have the similar grain (bulk) resistance, but the grain-boundary resistances in YSZ and LSO are also much higher than those in the YSZ-LSO composite ceramics. Meanwhile, at 500 ℃ as shown in Fig. 3(c), the complex impedance plots of YSZ-LSO composite samples exhibit only two arcs, which correspond to the grain-boundary effect and electrode effect, respectively. The grain effect could not be detected for the limited frequency. While the contribution from grain, grain boundary and electrode can still be seen obviously in the LSO single phase sample. These results indicate that the composite process has improved obviously the grain boundary conductivity at 300 ℃ and 400 ℃.

Figure 4 shows Arrhenius plots of the four kinds of oxide-ion conductors. It can be seen that the YSZ-6LSO composite ceramic has the highest conductivities in the test temperature range. The conductivities of the YSZ-6LSO and YSZ-4LSO composite ceramics are 0.215 S/cm and 0.158 S/cm, respectively, at 700 ℃. The conductivity of the YSZ-6LSO is three times in magnitude higher than that of the YSZ (0.062 S/cm) single phase and has two orders in magnitude higher than that of the LSO (0.0014 S/cm) single phase at 700 ℃. These indicate that composite technology with a little amount LSO is one of the efficient processes to improve the conductivity of the YSZ oxide-ion conductors.

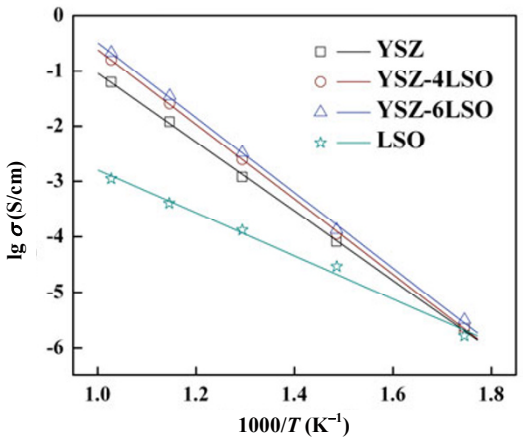

Fig. 4 Temperature dependence of conductivity in Arrhenius plots of the studied samples.

As shown in Fig. 3 and Fig. 4, YSZ-4LSO and YSZ-6LSO composite ceramics have much higher conductivities than the single phase YSZ and LSO ceramics. The high conductivity of the composite materials could not originate from the YSZ and LSO phases themselves, some factors from the compositing effect such as interfacial effect should play a key role for the conductivity enhancement. As shown in Fig. 3, for the similar sample size, all the samples have the similar grain contribution to conductivity, but the YSZ-LSO composites show better grain-boundary conductivities.

3.3 Discussion

In order to evaluate the interfacial effect originated from the compositing process, the relationships between the impedance and frequency, and between the modulus and frequency, were analyzed. Figure 5 shows the impedance-frequency and modulus-frequency plots for YSZ, YSZ-4LSO and YSZ-6LSO samples at 300 ℃, 400 ℃ and 500 ℃, respectively. Where, M'' is the imaginary part of complex electric modulus, Z'' is the imaginary part of complex impedance, and f is the frequency. In order to present the variation tendency of M'' and Z'' with the increasing of frequency, the scaled to its maximum modulus and impedance, M''/M''_{max} and Z''/Z''_{max}, are used in Fig. 5.

In Fig. 5(a), the impedance-frequency and modulus-frequency plots for YSZ, YSZ-4LSO and YSZ-6LSO samples, at 300 ℃, were drawn. Two Z''/Z''_{max} peaks relating to the grain effect at high frequency range and the grain-boundary effect at intermediate frequency region can be seen for the three samples, and one M''/M''_{max} peak is found in the modulus-frequency plots for all the samples. It is found that the Z''/Z''_{max} peaks at higher frequency almost overlap with their M''/M''_{max} peaks in the YSZ-LSO composite ceramics, while the Z''/Z''_{max} peak at higher frequency for YSZ separates from its M''/M''_{max} peak. Generally, the conductive mechanism is considered to be the localized relaxation process if the impedance peak separates from that of the modulus, and the

conduction process change from the localized relaxation process to a long-range conduction process when the peaks of impedance and modulus coincide or overlap each other [19]. So, it could be concluded that the conduction in YSZ dominates by the localized relaxation process at 300 ℃. In the YSZ-LSO composite ceramics, the impedance peaks of the grain effect overlap with the plot peaks of modulus, implying that the long range conduction in grains dominates the conductive process.

When the temperature increases, all the impedance-frequency and modulus-frequency peaks shift toward the higher frequency region. Figure 5(b) shows the modulus and impedance to frequency plots obtained at 400 ℃. All peaks shift toward higher frequency region at least by one order in magnitude, comparing to those measured at 300 ℃. For the frequency limitation of the measurement system, the M''/M''_{max} peaks and the higher-frequency Z''/Z''_{max}peaks in the plot could not be detailed at 400 ℃, although the tendency shift to higher frequency could be observed. From the tendency, one can see that the higher-frequency Z''/Z''_{max} plot overlap the M''/M''_{max} plot at 400 ℃ for all three samples. This shows that the conductive way is transformed into long range conductivity. The higher Z''/Z''_{max} frequency peak and lower one almost overlap each other in the samples at 500 ℃ (shown in Fig. 5(c)). The grain-boundary effect and the grain effect can not be distinguished from the Z''/Z''_{max} plot, indicating that the grain boundaries and the grains have similar conductivity.

As shown in Fig. 5, the composite materials have

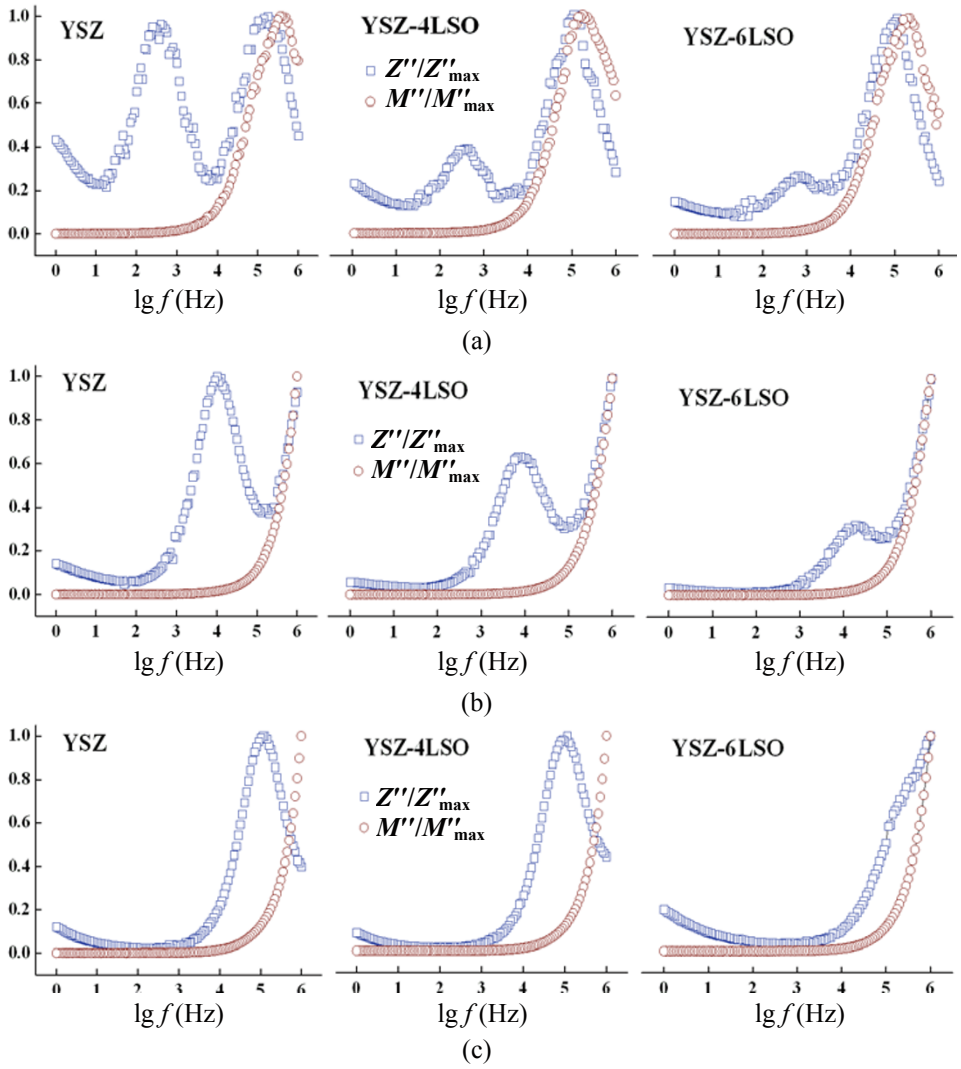

Fig. 5 Z''/Z''_{max} and M''/M''_{max} as a function of logarithmic frequency of YSZ ceramic and YSZ-LSO composites at temperatures of (a) 300 ℃, (b) 400 ℃ and (c) 500 ℃.

higher frequencies (relaxation frequency, *f*) for the grain-boundary peak in the Z''/Z''_{max} plots than the YSZ single phase has at the same measurement temperatures. In the case of a series connection of parallel *RC* component based on the simple brick model, the relaxation frequency can be expressed as:

$$f = \frac{1}{2\pi RC} \tag{1}$$

$$\sigma = L/AR \tag{2}$$

$$C = \varepsilon A/L \tag{3}$$

where *R* is grain boundary resistance, *C* is the capacity, *L* is sample thickness, *A* is the electrode area, σ is conductivity and ε is dielectric constant. Using Eq. (2) and Eq. (3) to replace corresponding items in Eq. (1), we have

$$f = \frac{\sigma}{2\pi\varepsilon} \tag{4}$$

Equation (4) indicates that the relaxation frequency *f* is determined by the conductivity σ and dielectric constant ε, although we can not calculate directly the conductivity by using the measured relaxation frequency *f* from Eq. (1), because the equivalent circuit should consist the other element such as constant phase element (CPE) for the impressed arcs as shown in Fig. 3. Since the dielectric constants ε of ionic conductors do not have much difference with each other, e.g. both the ε of YSZ and LSO are about 30 at room temperature [20,21], so the higher relaxation frequency *f* should be relate to the higher conductivity. This indicates that the composite materials have higher conductivity comparing to the single phase YSZ.

Generally, the conductivity of a material is determined by the concentration and transport rate of the charger carriers. The related relationship can be expressed as the following equation

$$\sigma = nq\mu \tag{5}$$

where *n* is the concentration of the charger carriers, *q* is the charge number of a charger carrier, and μ is a transport rate of the charger carriers. The charger carrier concentration is related to the defect number, *N*, in unit volume, as given in Eq. (6). For the oxygen ionic conduction, the defects are oxygen vacancies.

$$n = N\exp\left(-\frac{E}{2kT}\right) \tag{6}$$

where *E* is formation energy of a vacancy, *k* is Boltzmann constant and *T* is the absolute temperature. The XRD analysis shows that the lattice parameter of YSZ phase is *a*=0.5139 nm, and the ones of the LSO phase are *a*=0.9713 nm, *c*=0.7186 nm. The much different lattice parameters result in serious interfacial mismatch between YSZ and LSO, and result in the generation of dislocations. Defects like oxygen vacancies may be gravitated to the region of dislocations, which, in consequence, elevates the concentration of carriers in the YSZ-LSO composite materials than those in the YSZ and LSO single phases.

According to Maxwell-Boltzmann distribution law, the transport rate of a charger carrier along the electrical field can be determined as the following equation

$$\mu = \frac{q\delta^2\nu}{6kT}\exp\left(-\frac{U}{kT}\right) \tag{7}$$

where δ is the jump distance that is lattice parameter of the conductor, ν is the vibration frequency of the charger carriers, *U* is the periodic potential of crystal lattice, the other symbols have the same meaning as defined in Eq. (5) and Eq. (6). When an oxygen ion has energy higher than the *U*, the oxygen ion can exchange the lattice site with an oxygen vacancy locating around it, contributing to the charge carrier transport. By combining Eqs. (5), (6) and (7), the conductivity expressed in Eq. (5) can be described as Eq. (8)

$$\sigma = N\exp\left(-\frac{E}{2kT}\right)\frac{q^2\delta^2\nu}{6kT}\exp\left(-\frac{U}{kT}\right) \tag{8}$$

Here, one can get that the conductivity of the oxygen ionic conductors is mainly determined by the defect number *N,* if we assume that all the conductors in present work have the similar *E*, *q*, δ, ν and *U* at the same temperature. For the YSZ-LSO composite materials, the serious interfacial mismatch results in: (1) much more lattice defects at the interfaces, indicating higher charger carrier concentration in the composite materials than those in the single phases; (2) higher local lattice energy, showing the higher transporting ability of the charger carrier at the interfaces. This means that the composite materials could have higher conductivities.

4 Conclusions

The nanometer powders of YSZ, LSO have been prepared by using a modified coprecipitation method, and the YSZ-LSO composite materials with the weight ratios of 4 wt% LSO and 6 wt% LSO were obtained, respectively. The average sub-grain sizes of the as-sintered composite ceramics are around 200 nm.

The conductivity of the composite materials YSZ-6LSO is 0.215 S/cm at 700 ℃. The conductivity of this composite is three times higher than that of the polycrystalline YSZ and has two orders in magnitude higher than that of the polycrystalline LSO at 700 ℃. The conductivity of YSZ composite ceramic has been improved obviously by the composite technology. The interfacial effect of the composite materials plays a key role for the conductivity enhancement. Comparing to the single phase YSZ, the serious interfacial mismatch in the YSZ-LSO composite materials produces much more lattice defects and higher local lattice energy at the interfaces, resulting in higher charger carrier concentration and higher transporting ability of the charger carrier at the interfaces. The composite technology is expected to have extensive technological applications in conductivity improvement of the electrolyte for the intermediate temperature solid oxide fuel cells.

Acknowledgement

The authors acknowledge the support of the National Nature Science Foundation of China (Nos. 50872155 and 51172287). Much thanks to Dr. Haitao ZHOU for his useful information about this work. The first author also acknowledges the close discussion with Mr. Kaiming ZHANG and Mr. Hui YU.

References

[1] Steele BCH. Fuel-cell technology: Running on natural gas. *Nature* 1999, **400**: 619-621.

[2] Zhang H, Zhang Z, Ma GQ, *et al.* Copercipitation synthesis and oxide onic conductivities of $Ce_{0.8}Sm_{0.2}O_{1.9}$ based nanocomposite materials. *J Inorg Mater* 2009, **24**: 353-356

[3] Sanna S, Esposito V, Tebano A*, et al.* Enhancement of ionic conductivity in Sm-doped ceria/yttria-stabilized zirconia heteroepitaxial structures. *Small* 2010, **6**: 1863-1867.

[4] Azad SM, Wang OA, Saraf CM, *et al.* Nanoscale effects on ion conductance of layer-by-layer structures of gadolinia-doped ceria and zirconia. *Appl Phys Lett* 2005, **86**: 131906-131908.

[5] Souza F. Sol-gel nonhydrolytic synthesis of a hybrid organic-inorganic electrolyte for application in lithium-ion devices. *Solid State Ionics* 2004, **166**: 83-88.

[6] Garcia-Barriocanal J, Rivera-Calzada A, Varela M*, et al.* Colossal ionic conductivity at interfaces of epitaxial ZrO_2:Y_2O_3/$SrTiO_3$ heterostructures. *Science* 2008, **321**: 676-680.

[7] Sillassen M, Eklund P, Pryds N, *et al*. Low-temperature superionic conductivity in strained yttria-stabilized zirconia. *Adv Funct Mater* 2010, **20**: 2071-2076

[8] Reyren N, Thiel S, Caviglia AD, *et al.* Superconducting interfaces between insulating oxides. *Science* 2007, **317**: 1196-1199.

[9] Li S, Li ZC, Bergman B. Lanthanum gallate and ceria composite as electrolyte for solid oxide fuel cells. *J Alloy Compd* 2010, **492**: 392-395.

[10] Xu D, Liu XM, Wang DJ, *et al.* Fabrication and characterization of SDC-LSGM composite electrolytes material in IT-SOFCs. *J Alloy Compd* 2007, **429**: 292-295.

[11] Chockalingam R, Chockalingam S, Amarakoon VRW. The electrical properties of microwave sintered gadolinia doped ceria-alumina nano-composite electrolyte. *J Power Sources* 2011, **196**: 1808-1817.

[12] Mizutani Y, Tamura M, Kawai M. Development of high-performance electrolyte in SOFC. *Solid State Ionics* 1994, **72**: 271-275.

[13] Wang Q, Peng R, Xia C, *et al.* Characteristics of YSZ synthesized with a glycine-nitrate process. *Ceramics International* 2008, **34**: 1773-1778.

[14] Tolchard JR, Slater PR, Islam MS. Enhanced ionic conductivity in $Ce_{0.8}Sm_{0.2}O_{1.9}$: Unique effect of calcium co-doping. *Adv Funct Mater* 2007, **17**: 2847-2854.

[15] Guo C, Cai T, Zhang W, *et al*. Synthesis and characterization of Al^{3+}-doped $La_{9.33}Ge_6O_{26}$ intermediate temperature electrolyte for SOFCs. *Mater Sci Eng B* 2010, **171**: 50-55.

[16] Zhang H, Li ZC, Bergman B, *et al*. Investigation of $La_{9.33}Si_6O_{26}$ oxygen ionic conductor. *J Mater Sci Tech* 2007, **23**: 629-632.

[17] Chefia S, Madani A, Boussetta H, *et al*. Electrical properties of Al-doped oxyapatites at intermediate temperature. *J Power Sources* 2008, **177**: 464-467.

[18] Tian CG, Liu JL, Cai J, *et al*. Direct synthesis of $La_{9.33}Si_6O_{26}$ ultrafine powder via sol-gel self-combustion method. *J Alloys Compd* 2008, **458**: 378-382.

[19] Gerhardt R. Impedance and dielectric spectroscopy revisited: Distinguishing localized relaxation from long-range conductivity. *J Phys Chem Solids* 1994, **55**: 1491-1506.

[20] Henn FEG, Buchanan RM, Jiang N, *et al*. Permittivity and AC conductivity in yttria-stabilized zirconia. *Appl Phys A* 1995, **60**: 515-519.

[21] Copel M, Cartier E, Ross FE. Formation of a stratified lanthanum silicate dielectric by reaction with Si(001). *Appl Phys Lett* 2001, **78**: 1607-1069.